



HAL
open science

**Robust grid-oriented control of high voltage DC links
embedded in an AC transmission system International
Journal of Robust and Nonlinear Control †**

L Arioua, B Marinescu

► **To cite this version:**

L Arioua, B Marinescu. Robust grid-oriented control of high voltage DC links embedded in an AC transmission system International Journal of Robust and Nonlinear Control †. International Journal of Robust and Nonlinear Control, 2016, 26, pp.1944 - 1961. hal-01450076

HAL Id: hal-01450076

<https://hal.science/hal-01450076v1>

Submitted on 17 Mar 2020

HAL is a multi-disciplinary open access archive for the deposit and dissemination of scientific research documents, whether they are published or not. The documents may come from teaching and research institutions in France or abroad, or from public or private research centers.

L'archive ouverte pluridisciplinaire **HAL**, est destinée au dépôt et à la diffusion de documents scientifiques de niveau recherche, publiés ou non, émanant des établissements d'enseignement et de recherche français ou étrangers, des laboratoires publics ou privés.

Robust grid-oriented control of high voltage DC links embedded in an AC transmission system

L. Arioua^{1,2} and B. Marinescu^{1,2,*†‡}

¹RTE R&D Division, 9 rue de la Porte de Buc, Versailles, 78000, France

²SATIE Laboratory, Ecole Normale Supérieure de Cachan, 61, avenue du Président Wilson, Cachan, 94230, France

SUMMARY

Several studies have shown that the way to design controllers for the high-voltage direct current (HVDC) links impacts the transient behavior of the electric system in which the latter are inserted. This can be exploited to improve the performances of the stability of the power system. In this paper, a robust multi-variable control design for the converters of an HVDC link is proposed. It is based on the coordination of the control actions of the HVDC converters and the use of a control model. The latter takes into consideration, in addition to the dynamics that mostly impact the stability of the neighbor zone of the HVDC link, several cases of faulted situations modeled as uncertainties. An H_∞ controller allowed us to achieve robustness against such uncertainties. The new controller is tested in comparison with the standard vector control and an optimal linear quadratic controller using the EUROSTAG simulation software (Tractebel Engineering, Brussels, Belgium and Réseau de Transport d'Électricité (RTE) - France) on both academic and realistic large-scale power systems. Copyright © 2015 John Wiley & Sons, Ltd.

Received 19 March 2014; Revised 11 April 2015; Accepted 6 June 2015

KEY WORDS: HVDC; transient stability; H_∞ control; output-feedback control

1. INTRODUCTION

The high-voltage direct current (HVDC) link is a mean of transmission of electric power based on high-power electronics. During the last decades, this kind of power transmission has obtained great attention. In fact, many projects of insertion of HVDC links are undergoing. Because of its rapid responses and flexibility, the HVDC technology is able to provide to the transmission system advantages as transfer capacity enhancement and power flow control [1]. Initially, it was used to interconnect two asynchronous systems. In this case of use, the ends of the HVDC link are electrically independent, which avoids the propagation of perturbations (like, e.g., faults) between the two alternating current (AC) areas. This is, for instance, the case of the England–France interconnection [2]. Nowadays, HVDC links are more and more inserted into the same AC power system in parallel with other existing AC lines and other dynamic elements as generators. In this new context of use where the HVDC is embedded in a meshed AC system, all the elements are in interaction, and the stability of the neighbor zone of the HVDC link may be influenced by these interactions. This conducted us to find a way to take into consideration the aforementioned interactions during the control law synthesis. A new kind of mode—called electrical coupling mode—was put into evidence. It involves dynamics of distant machines, and it is different from a well-known inter-area mode. These new interactions allowed us to better identify the machines responsible for the transient stability of the neighbor zone of the HVDC link. This information was exploited to provide a new type of control model. This new context of use of the HVDC links motivated several studies, which confirm

*Correspondence to: B. Marinescu, RTE R&D Division, 9 rue de la Porte de Buc, Versailles, 78000, France.

†E-mail: Bogdan.Marinescu@ircyn.ec-nantes.fr

‡Present address: IRCCyN-Ecole Centrale Nantes, 1, rue de la Noë, FR-44321 Nantes Cedex 3.

that the way to control the HVDC converters impacts the stability of the system in which the link is embedded [3–8]. Several controller schemes have been proposed to enhance the dynamic performances of the neighbor zone of the HVDC link. In [9, 10], for instance, the control of the HVDC converters is developed on the base of the model of the whole power system, but this approach is not possible for large-scale power systems. Indeed, the major difficulty encountered during the control law synthesis is the way to take into account the rest of the power system. In [11], for example, a coordinated controller based on on-line identification of the power system parameters has been developed. In [12, 13], controllers for HVDC converters using remote information from generators are proposed. In [14], an adaptive optimal controller was synthesized using real-time system-wide measurements. In the approaches cited previously, even if the rest of the power system is taken into account, the use of remote data is unavoidable. These latter are not always available at the converters' stations, which limits the application of these methods. This conducted us to focus on the way to take into consideration the power system according to the given grid objectives using only variables available at converter stations. For this, an adequate control model is proposed and next used for the synthesis of the regulators of the HVDC link.

This paper presents thus a new method for developing a control model based on the analysis of the AC power system and particularly the AC zone surrounding the HVDC link. This analysis allowed us to determine the main dynamics impacting the power system stability. Moreover, in order to better capture the power system variations during a fault, critical faulted situations are considered during the synthesis. This led us to use a more efficient robust control design based on the H_∞ theory.

The paper is organized as follows: In Section 2, the analysis of the different interactions that exist in the neighbor zone of the HVDC is presented, which allowed us to develop the nominal nonlinear control model in Section 3. Section 4 is dedicated to the synthesis of the uncertain linear model. The latter is used in Section 5 to develop a robust multivariable output-feedback controller for the HVDC converters. Finally, in Section 6, simulation results are presented to illustrate the performances and robustness of the new control strategy in comparison with those of standard ones.

2. ANALYSIS OF THE NEIGHBOR ZONE OF THE HIGH-VOLTAGE DIRECT CURRENT

We are focusing on the stability of the neighbor zone of the HVDC link. For this reason, we analyze the different interactions that exist between the different power system dynamic elements. As it is explained later, these interactions affect the stability of the power system especially when a severe fault (short circuit, loss of a group, etc) occurs.

2.1. Power system stability problem

The stability of a power system may be broadly defined as its property to reach an equilibrium point after a disturbance as, for instance, a short circuit. Depending on whether the perturbations caused by the fault are small or large, we speak about small-signal stability or, respectively, transient stability. One of the main concerns in both cases is the loss of synchronism of one or more generators. That is, the frequency of some generators of the grid cannot reach the equilibrium value (50 Hz in Europe) after a disturbance.

Small-signal stability [15]. It is the ability of the power system to maintain synchronism under small disturbances such as small variations of loads and generation. The disturbances are considered sufficiently small to allow the use of the linear approximation of the dynamic system equations. The instability that may results can be of two forms: steady increase in rotor angle due to lack of sufficient synchronizing torque or rotor oscillations of increasing amplitude due to lack of sufficient damping torque. In today's power systems, small-signal stability is largely a problem of insufficient damped oscillations. The stability of the following types of oscillations is studied through the modal analysis of the linear approximation model. More specifically, this is reflected by two kinds of modes:

- Local modes related to the swing of a generator against the rest of the power system.
- Inter-area modes related to the swing of several machines in one part of the system against another group of machines in another part of the system.

Transient stability [15]. It is the ability of the power system to maintain synchronism when subjected to a severe transient disturbance like, for instance, short circuits. The system response to such a disturbance involves large excursions of generator rotor angles because of the nonlinear power–angle relationship. Stability will then depend on both the operating state of the system at the time when the disturbance is applied and the severity of the disturbance. In the case of short circuits, the degree of stability is quantified by the so-called critical clearing time (CCT), which is defined as the maximal fault duration at a given location for which the system remains transiently stable [15]. Thus, the CCT is a margin of stability of the power system.

More specifically, a short circuit systematically leads to two types of topology variations. The first one corresponds to the modification of the entries of the grid admittance matrix, which correspond to the branches impacted by the fault. The second one corresponds to the fault clearing (if the fault was on a branch, the clearing is performed by the trip of the branch). The latter topology modifications can be easily captured into a linear model of the dynamic power system equations. However, because the power system is nonlinear, the final post disturbance and, thus, the CCT depend not only on these topology variations.

Impact of the high-voltage direct current link on the system transient stability. Studies of the HVDC link inserted in a power system have investigated the impact of the HVDC on the transient stability and the small-signal stability of its neighbor zone. In [6], for instance, the author shows that the enhancement of the overall system dynamic performance of the neighbor zone of the HVDC link is possible by minor modifications in the HVDC controls. In [16], the transient stability of the neighbor zone of the HVDC link is assessed for different direct current (DC) power levels, which indicates how the HVDC transmission can increase the CCT at several locations of the neighbor zone.

2.2. Electrical interactions and critical clearing time

Part of the electrical interactions that impact the transient stability can be described by several types of modes. This is illustrated on the following example.

Example of application

Consider the simplified representation of the France–Spain–Portugal zones introduced in [17], which consists of 23 machines as shown in Figure 1. The system is represented by a detailed nonlinear model including generators along with their regulations. Only the high-voltage network (225 and 400 kV) is modeled. The interconnection between France and Spain, which consists of four AC lines, is reinforced by adding a voltage source converter (VSC)-based HVDC link of 65-km length with a nominal active power of 1000 MW and a rated pole voltage of ± 320 kV.

The interconnected power system is analyzed here for the perspective of the control of the HVDC. Thus, the open-loop input–output system defined by the controls U and measures y chosen for the control of the converters of the HVDC should be considered (this model is described in detail in Section 4.1 by Σ_{NL} in (3)). When linearized as explained in Section 4.1, a linear state-space form Σ_L (given further on by (4)) is obtained. The singular values of the transfer matrix of Σ_L presented earlier are given in Figure 2. Two poorly damped modes are visible, and their characteristics are given in Table I.

The modal analysis of the whole system showed that the mode 1 is an inter-area mode. As a matter of fact, the states with higher participation in this mode are related to rotor dynamics (Table I). As recalled in Section 2.1, this kind of mode is due to the electrical coupling of geographically distant generators. It is thus of interest to quantify the impact of the HVDC on the stability of its neighbor zone.

The second mode in Table I is not of inter-area nature because the states with higher participation in this mode are not associated to rotors but to D-axes. It is thus an electrical mode. However, notice

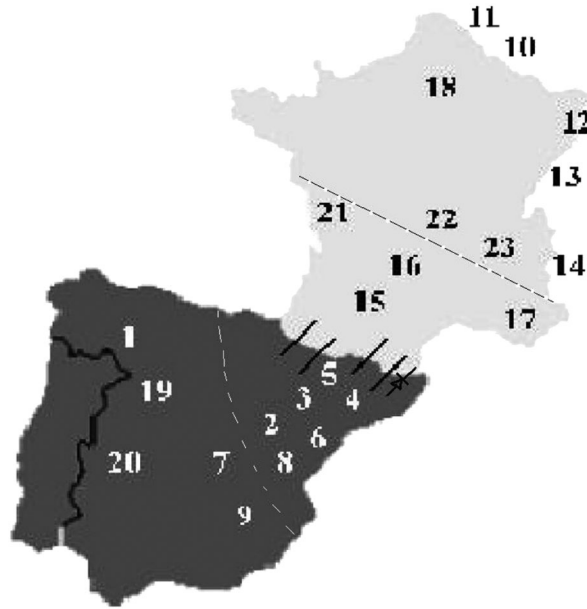


Figure 1. France–Spain–Portugal interconnected systems.

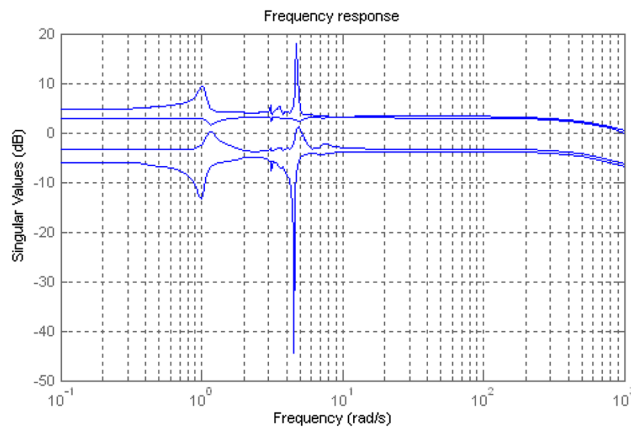


Figure 2. Frequency response of the nominal model.

Table I. Machines with the highest participation in modes 1 and 2.

	Machines with major participation	f [Hz]	Rotor participation	D-axis participation
Mode 1	G15	0.64	0.23	0.0035
	G23		0.21	0.003
Mode 2	G19	0.16	0.38	0.41
	G1		0.0063	0.038

that, as shown in Table I, several machines have important participations in this mode. This means that this kind of mode, although it is not of electromechanical nature as the inter-area ones, is also due to electrical coupling of distant machines and thus of interest for the analysis of the transient stability of a zone. This new type of mode is called in the sequel an *electrical coupling mode*. Indeed, to further investigate this aspect, consider that the benchmark of Figure 1 for which the impedance of a line is directly connected to machine G_{19} (which is highly participating in mode 2, Table I) is varied. Table II shows that there is a direct correlation between the length of this line, the damping of mode 2, and the CCT computed at the terminal bus of G_{19} .

Table II. Correlation between the length of the line, the damping of mode 2 and the CCT.

Impedance of the line [pu]	Damping of the mode 2	CCT [ms]
0.50	3.58	28
0.36	6.39	29
0.036	17.89	32
0.012	21.57	37

CCT, critical clearing time.

Table III. Selected critical machines.

Gen (Fr)	CCT [ms]	Gen (Sp)	CCT [ms]
G16	64	G2	178
G15	203	G8	179
G17	205	G5	214
G21	280	G6	235

Table IV. Machines with the highest participation in the poorly damped coupling modes.

Modes	Damping of mode	Machine kept
1	3.26	G_{15}
2	6.40	G_{19}

3. THE NOMINAL NONLINEAR CONTROL MODEL

A full large-scale simulation model of the interconnected power system is usually available and currently updated by the transmission system operators (TSOs) (e.g., [18, 19]). We have chosen to use this kind of full model to extract a control model. The objective of this latter model is to capture the dynamics that may impact the transient stability and that have the greatest impact on the neighbor zone of the HVDC link.

3.1. Machine selection strategy

First, as it has been explained in Section 2, the CCT is a good indicator of the transient stability level of the HVDC link neighboring zone. Therefore, the strategy of machine selection adopted in this paper is based on the computation of CCTs at well-chosen points of the neighbor zone. These points are determined by *a priori* stability studies (usually carried out by TSOs). To each case of fault, it associated the first machine, which loses synchronism and the corresponding CCT. The lowest values, which are situated under a chosen threshold, indicate the machines to be kept for the control model. At this stage, the machines kept for the example in Figure 1 are presented in the Table III.

Second, in Section 2.2, it has been shown that two classes of coupling modes are connected with transient stability. They provide information about distant devices that impact the stability of the neighbor zone. The list of chosen machines for the control model made previously based on local (CCT) considerations must thus be enriched by the most participating machines in the poorly damped aforementioned coupling modes. This allowed us to identify the machines illustrated in Table IV.

Thus, the final list of retained machines is the list of Table III plus G_{19} .

3.2. Network reduction

The topology is also reduced. More precisely, the buses to which the retained machines are connected are kept along with the end buses of the interconnections of interest (the HVDC link ones

and the neighbor AC zone ones). The rest of the buses and branches are replaced by a WARD-PV method [20], that is, by equivalent impedances and injectors.

3.3. Model of the high-voltage direct current link

A VSC-based HVDC is considered as in Figure 3(a). The converters are VSC employing insulated-gate bipolar transistor power semiconductors, one operating as a rectifier and the other as an inverter. The two converters are connected through a DC cable. These converters have the ability to rapidly control the transmitted active power and also to independently exchange reactive power with the AC system at each end. The high-frequency switching operation of the power electronics is neglected, and each converter can be considered as an ideal sinusoidal voltage source whose magnitude U_c and phase angle θ can be controlled [21]. The VSC-HVDC is thus modeled as two sources, each one in series with the converter transformer (see Figure 3(b), where $\bar{U}_{c1} = U_{c1i} + jU_{c1j}$, $\bar{U}_{c2} = U_{c2i} + jU_{c2j}$ and θ_1, θ_2 are respectively the magnitudes and the phase angles of the voltage sources. U_1 and U_2 are the AC voltages at the buses where the two HVDC converters are connected. P_1, P_2 and Q_1, Q_2 are respectively active and reactive powers exchanged with the power system, and $X_{T,1}, X_{T,2}$ are the transformer reactances). In this model of HVDC, it is assumed that the DC voltage is kept close to its rated voltage, because the dynamic imposed by its regulation is usually much faster than the one of currents. Therefore, the losses of the converters are assumed constant, regardless of the current through the converters. They are represented as a constant active load [21].

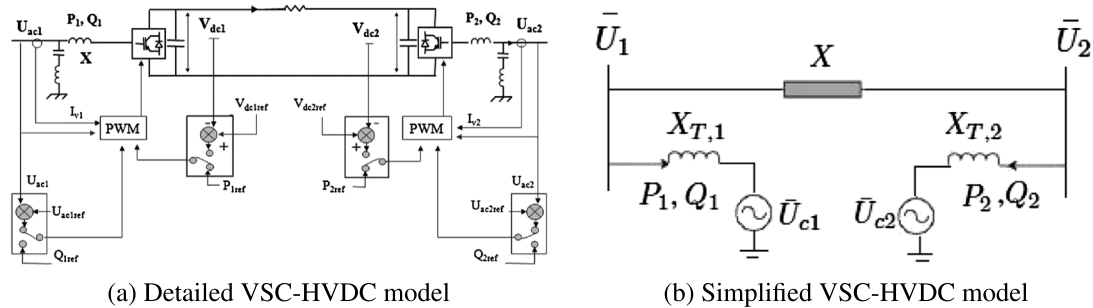


Figure 3. Voltage source converter-based high-voltage direct current (VSC-HVDC) link.

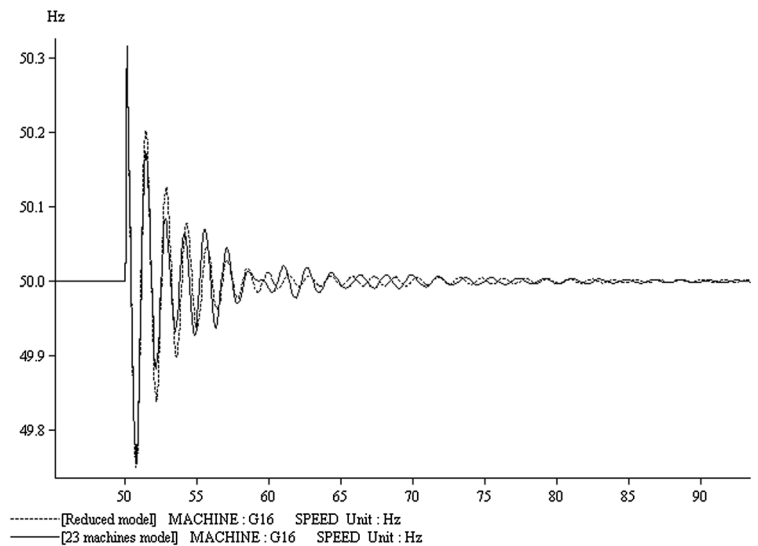


Figure 4. Speed of G_{16} obtained with the full and control model.

This leads to

$$\begin{aligned}
 P_1 &= (U_1(\sin \theta_1 U_{c1i} - \cos \theta_1 U_{c1j}))/X_{T1}, \\
 Q_1 &= (U_1^2 - U_1(\cos \theta_1 U_{c1i} + \sin \theta_1 U_{c1j}))/X_{T1}, \\
 P_2 &= (U_2(\sin \theta_2 U_{c2i} - \cos \theta_2 U_{c2j}))/X_{T2}, \\
 Q_2 &= (U_2^2 - U_2(\cos \theta_2 U_{c2i} + \sin \theta_2 U_{c2j}))/X_{T2}.
 \end{aligned}
 \tag{1}$$

In addition, notice that $P_2 = -P_1$. The control variables can be expressed as follows:

$$\begin{aligned}
 U_{c1i} &= U_{c1i0} + \Delta U_{c1i}, U_{c1j} = U_{c1j0} + \Delta U_{c1j}, \\
 U_{c2i} &= U_{c2i0} + \Delta U_{c2i}, U_{c2j} = U_{c2j0} + \Delta U_{c2j}.
 \end{aligned}
 \tag{2}$$

3.4. Validation of the nominal nonlinear control model

Figure 4 shows the speed response of the generator G_{16} of the example considered in Section 2.2 to a fault obtained with the control model (dotted line) and, respectively, with the full 23-machine model (solid line). The two curves do not completely overlap but have the same shape, which guarantee the computation of quite similar CCTs with both models.

4. THE UNCERTAIN LINEAR CONTROL MODEL

4.1. Linear approximation of the nominal model

The control model described in Section 3 is nonlinear and can be generally represented by the nonlinear differential and algebraic equations

$$\Sigma_{NL} : \begin{cases} \dot{x} = f(x, U) \\ y = g(x, U), \end{cases}
 \tag{3}$$

where x represents the state variables (speeds, angles of machines, automatic voltage regulators, governors variables, etc.). The latter model (3) corresponds to the well-known differential-algebraic equations form used to analytically model power systems for transient stability analysis like, for example, in [22]. The control variables U are the magnitudes of the voltage sources (Section 3.3). The outputs y are the measures of active and reactive powers usually used for the converter controls [21], and y_{ref} are the control references.

This leads to $U = [U_{c1i}, U_{c1j}, U_{c2i}, U_{c2j}]$, $y = [P_1, Q_1, Q_2]$, $y_{ref} = [P_{ref1}, Q_{ref1}, Q_{ref2}]$.

Let

$$\Sigma_L : \begin{cases} \Delta \dot{x} = A \Delta x + B \Delta U \\ \Delta y = C \Delta x \end{cases}
 \tag{4}$$

be the linear approximation of (3) around a given equilibrium point (x_0, U_0, y_0) , where $\Delta x = x - x_0$, $\Delta U = [\Delta U_{c1i}, \Delta U_{c1j}, \Delta U_{c2i}, \Delta U_{c2j}]$, $\Delta y = y - y_0$ and A, B, C are constant matrices. The latter linear model is used in Section 5 for the synthesis of a robust linear control.

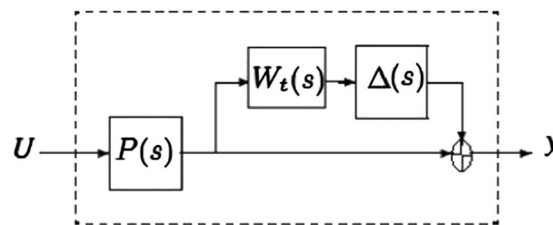


Figure 5. Plant with multiplicative output uncertainty.

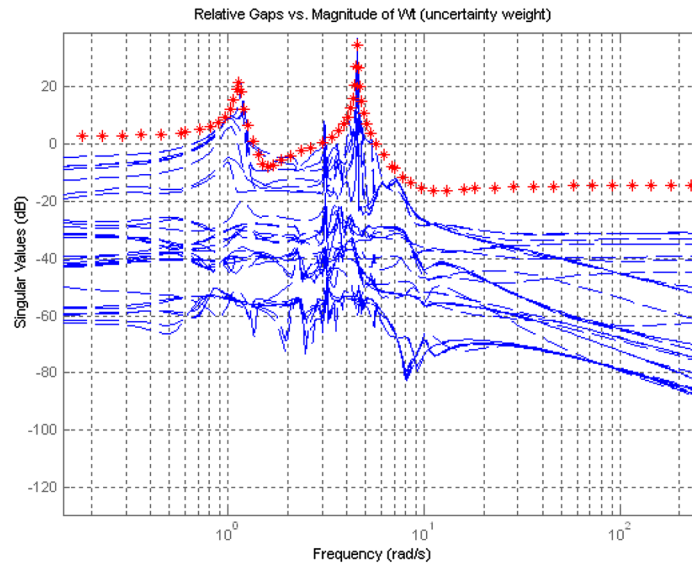


Figure 6. Relative error versus the magnitude of W_t .

4.2. Synthesis of the uncertain model

The two kinds of topology variation associated to a fault and explained in Section 2 can be directly taken into account in the linear approximation of the control model. Indeed, these different topologies generated during different cases of short circuits constitute a family of linear control models $P_\Delta(s)$, which can be considered as an unstructured uncertainty. The control model described in Section 3 is considered as the nominal model $P(s)$. More specifically, Figure 6 shows the singular values of the deviations $(P_\Delta(s) - P(s))P(s)^{-1}$ of all the aforementioned family of perturbed models with respect to the nominal one. The family of perturbed models generated is considered as an uncertain model $P_\Delta(s)$ with output unstructured uncertainty $P_\Delta(s) = (1 + \Delta(s)W_t(s))P(s)$ as shown in Figure 5, where $W_t(s)$ is the uncertainty weight. The latter weight is used to capture how the relative uncertainty varies with frequency, and it is chosen such that the maximum magnitude of all relative error curves in Figure 6 is below this weight. $\Delta(s)$ is the normalized model deviation with respect to the nominal model.

5. A ROBUST CONTROL DESIGN

5.1. Design requirements

The regulators of the HVDC converters are generally synthesized to ensure local performances as

- tracking of references for active and reactive powers $P_{\text{ref}1}$, $Q_{\text{ref}1}$, $Q_{\text{ref}2}$ or for voltages at both ends of the DC link according to the usual time setting for HVDC power control (time constants between 80 and 100 ms),
- possibility of inversion of the power flow in a given time (usually around 200 ms).

The control model developed earlier is used to synthesize a singular coordinated controller for both HVDC converters. This controller has to ensure the performances cited in the preceding texts in addition to the

- grid performances for several cases of fault (i.e., improvement of the transient stability).

Our control model includes the uncertainties that represent the different cases of critical situations (according to Section 4.2). This motivated the synthesis of a robust multivariable control.

Notice that, to avoid the use of remote variables (e.g., machines speed and angles), an output feedback structure is used for the control model.

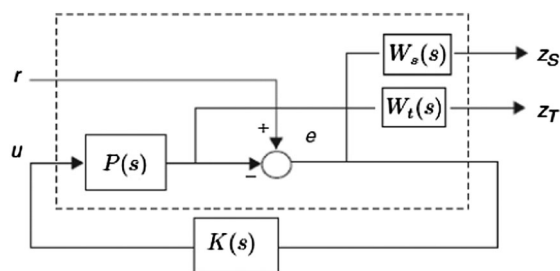


Figure 7. Plant with sensitivity weights.

Thus, only variables available at converter stations are used, and a coordinated controller is developed for both converters. Obviously, in case of use of remote signals, the performances of the control loop can be improved.

5.2. A mixed sensitivity H_∞ control design

We use the mixed sensitivity H_∞ control design. The sensitivity $S(s) = (I + P(s)K(s))^{-1}$ is the closed-loop transfer matrix from the reference inputs to the error (i.e., $r \mapsto e$ in Figure 7). The complementary sensitivity $T(s) = P(s)K(s)(I + P(s)K(s))^{-1}$ is the closed-loop transfer matrix from the references to the measured outputs (i.e., $r \mapsto Z_t$ in Figure 7), where $P(s)$ is the nominal model, $K(s)$ is the controller, and I is the identity matrix.

Let $W_t(s)$ be the weight used to achieve robustness against uncertainties caused by faulted situations as explained in Section 2 and $W_s(s)$ be another weight based on the desired shape of the sensitivity in order to satisfy the performances specified in Section 5.1. $W_s(s)$ is chosen in the form [23]

$$W_s = \left(\frac{s/\sqrt[k]{M_s} + \omega_b}{s + \omega_b \sqrt[k]{\varepsilon}} \right)^k, \tag{5}$$

where ω_b is the bandwidth, M_s is the peak sensitivity, ε is the steady-state error desired with respect to a step input, and k is the order of the weighting function. Notice that making ε small enforces the integral action (in our case $\varepsilon = 10^{-4}$).

The closed-loop system is guaranteed stable for all plants in $P_\Delta(s)$, if a controller $K(s)$, which ensures $\|W_t(s)T(s)\|_\infty \leq 1$ for all frequencies, is found [24]. The desired performances are achieved if $\|W_s(s)S(s)\|_\infty \leq 1$. Thus, the H_∞ controller $K(s)$ is designed to minimize the cost function:

$$\lambda = \left\| \begin{bmatrix} W_s(s)S(s) \\ W_t(s)T(s) \end{bmatrix} \right\|_\infty \leq 1. \tag{6}$$

The gain λ (defined by (6)) obtained is about 1.05. When the value of lambda is less or equal than 1, 100% of the desired performances are achieved. However, we assume that 1.05 is acceptable, and the frequency-domain tracking performance and robustness specified before are met by the controller $K(s)$.

5.3. Computation and implementation of the controller

The multivariable robust controller $K(s)$ is calculated by solving an associated Ricatti equation via a function of robust control toolbox of Matlab. The final controller is given in its state representation (A_K, B_K, C_K, D_K) , and it is of the same order as the linear control model augmented by the weights $W_s(s)$ and $W_t(s)$. In the case of the example of Section 2.2, the linear control model obtained after reduction and minimal realization is of order 30 (Appendix B). The controller obtained is of order 40, which is too high for implementation. For this reason, it is a common practice to reduce the order of the controller. A reduction method based on the singular values [23] allowed us to generate a controller of order 5. This method of reduction is based on the computation of the Hankel singular

values of the system, which indicate the respective state energy of the system. The reduced order can be directly determined by examining the system Hankel singular values. The truncations have been performed with an existing function in robust control design toolbox of Matlab named *reduce*.

6. SIMULATION TESTS

This section deals with the validation of the proposed controller. In fact, simulation tests using the EUROSTAG software (Tractebel Engineering, Brussels, Belgium and Réseau de Transport d'Electricité (RTE) - France) [22] are performed with both the 23-machine benchmark (Section 2.2) and a second one based on realistic large-scale model of the European power system. Notice that EUROSTAG is a software developed for accurate and reliable simulations of power system dynamics. It is used for the dynamic phenomena with time constants in the range from few milliseconds to a few seconds. It mainly concerns the problems of stability of groups in case of faults.

6.1. Description of the alternative controls

The new controller is compared with two other controllers. The first one is the standard vector controller, usually used in power systems for the control of power electronics (e.g., [25]). The proportional and integral gains of this control are synthesized using standard criteria for electrical drives to satisfy the performances specified in Section 5.2. The second controller is a coordinated optimal linear quadratic (LQ) controller (e.g., [26]); we have synthesized on the base of the linearized nominal model described in Section 3. The three controllers are tuned to satisfy almost the same local performance specifications. As a consequence, the robustness level they provide can be directly compared.

In what follows, the three controllers mentioned earlier are first tested on the 23-machine example of Section 2.2.

6.2. Local performances

An export of 1000 MW is considered from France to Spain via the HVDC link. To test local performances, a -0.1 -pu step is applied to the reference of the active power transmitted through the HVDC link (P_{ref1}). Figure 8 shows the responses of the active power. It can be noticed a good tracking of the active power reference and time constants compliant with the specifications given in Section 5.2. In addition, one can remark that the three controllers provide almost the same closed-loop dynamics.

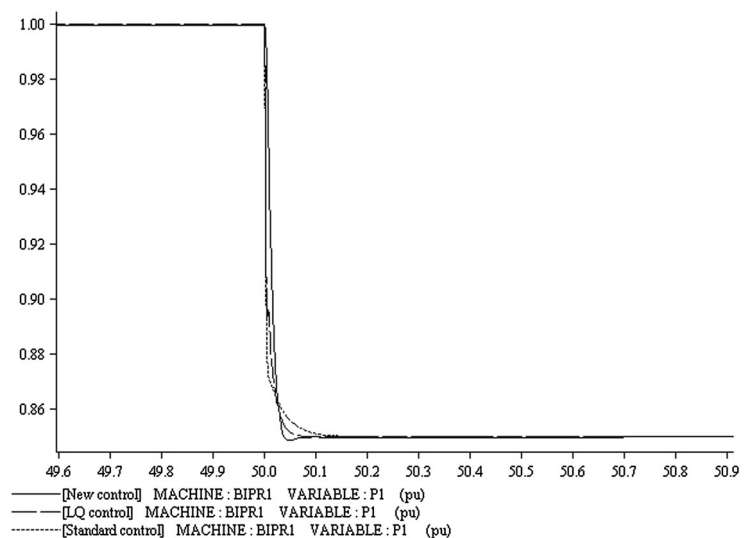


Figure 8. Response of P_1 to a -0.1 -pu step on P_{ref1} .

6.3. Transient stability

Figure 9(a) and (b) presents the active and reactive power responses to a symmetrical short circuit of 100 ms occurring near the converter 1 (French side). It can be seen better dynamic responses with the new H_∞ controller. In fact, a lower time of recovering after the fault and a lower overshoot are observed. This leads to less severe saturation in operation in comparison with the standard one. Furthermore, Figure 10(a) and (b) shows that the transient oscillations obtained with the H_∞ and the LQ controllers are more damped than the ones obtained with the standard vector control.

In addition to the simulations presented earlier, the CCTs obtained with the three controllers were compared in Table V. A difference up to 15% is observed between the use of the new controller and

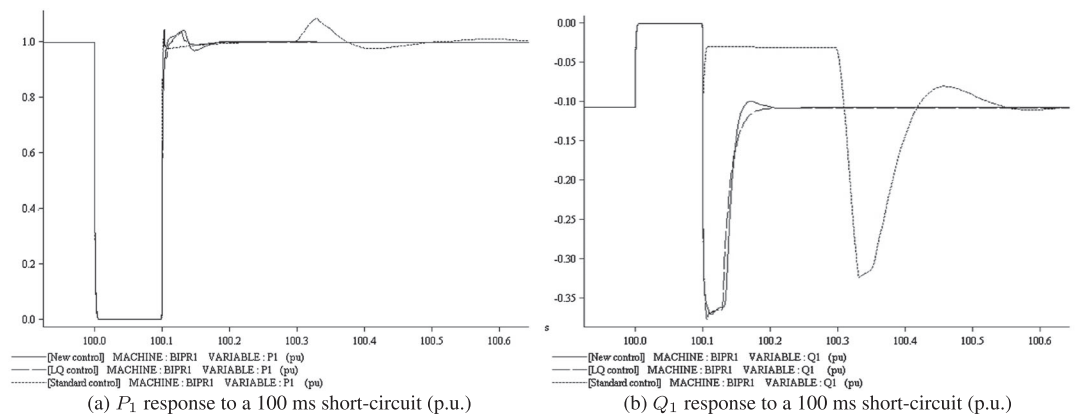


Figure 9. Active and reactive power responses to a 100-ms short circuit in case of 1000-MW power export.

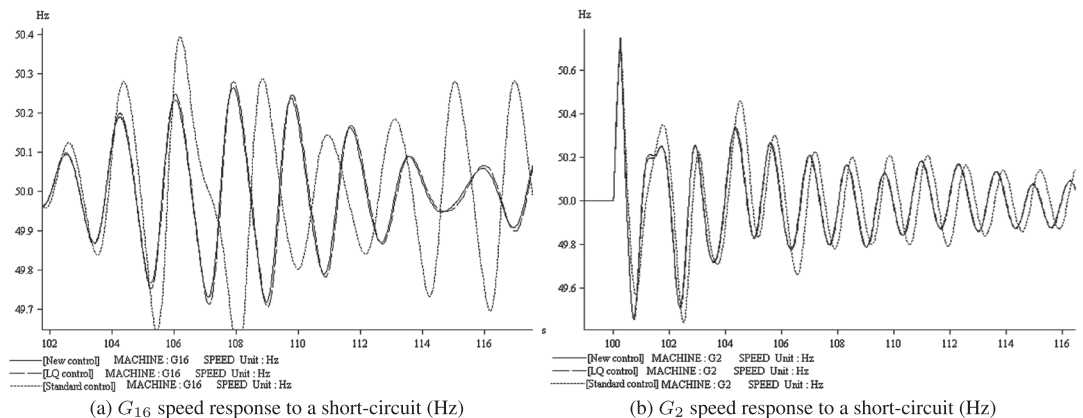


Figure 10. Machine responses to a short circuit in case of power export.

Table V. Critical clearing time validation of the new controller.

Location of the fault	Standard controller CCT [ms]	LQ controller CCT [ms]	New controller CCT [ms]
Llogaia	245	277	284
Vic	223	249	255
Bescano	212	239	246
Vandellos	127	130	137
Braud	138	140	161

CCT, critical clearing time; LQ, linear quadratic.

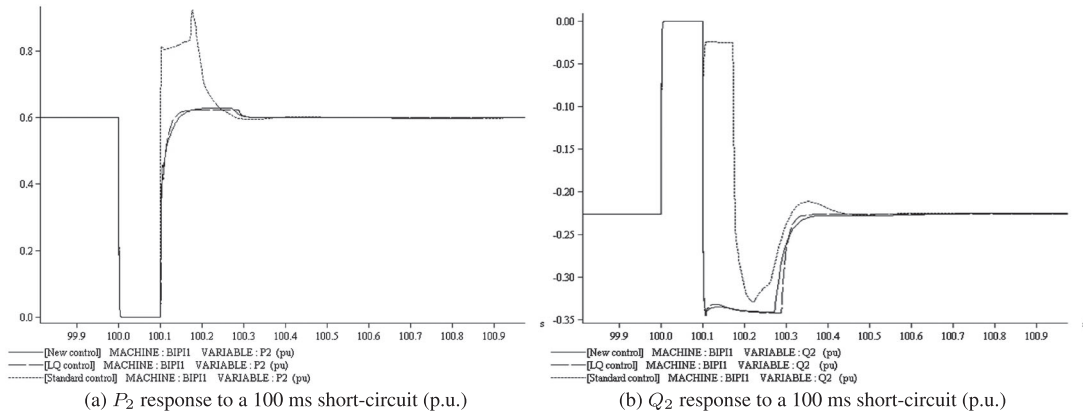


Figure 11. Active and reactive power responses to a 100-ms short circuit in case of 600-MW power import.



Figure 12. Insertion of the Midi-Provence high-voltage direct current (HVDC) link in the European interconnected power system.

the LQ controller and up to 23% between the new controller and the standard one. This confirms the improvement of transient stability in the case of the new robust H_∞ controller in comparison with the two other controllers.

6.4. Robustness against the variation of operating point

The robust proposed controller was synthesized using a linearized model. This conducts us to perform some additional tests of robustness of performances against the variation of the operating point. A new situation of load flow is considered for the simulations. The import from Spain to France is 600 MW in this case. Notice that the same controllers as before are used, that is, the ones synthesized using the export situation. Figure 11(a) and (b) gives the active power and reactive power responses to 100-ms short circuit applied near the converter 2 (Spanish side). Both are comparable with the ones obtained when the export scenario is used (Figure 9(a) and (b)). Moreover, in this situation also, the responses are better than the ones obtained with the standard and LQ controllers. This confirms the good robustness of the performances of the proposed controller against variation of operating conditions.

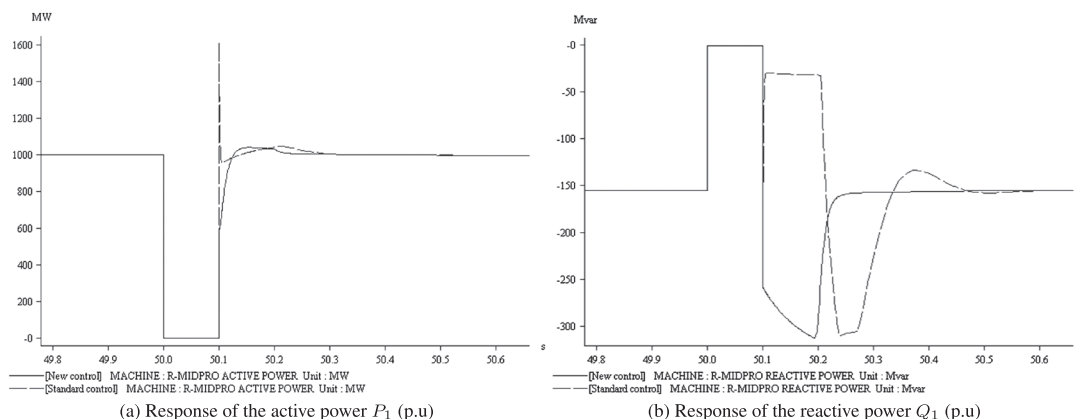


Figure 13. Responses to a 100-ms Tavel–Tamareau short circuit.

Table VI. Critical clearing time validation for the real European system.

Fault simulated	Standard controller CCT [ms]	Robust controller CCT [ms]
Darse-Feuillane	216	224
Feuillane-Ponteau	192	204
Ponteau-Feuillane	183	195
Ponteau-Realtor	181	192
Feuillane-Lavera	194	205

CCT, critical clearing time.

6.5. Tests on a realistic large-scale model of the European power system

The methodology developed in this paper was also applied to a realistic large-scale model of the European power system. This model is the one mentioned at the beginning of Section 3, and it is generally used for interconnection and reinforcement studies by the European TSOs. It is a detailed nonlinear model including generators along with their regulations (automatic voltage regulators, power system stabilizer, and governors) and where the high voltage network (225 and 400 kV) is modeled. It consists of 1121 generators, 7625 nodes, 10,404 lines, 2550 transformers, and 458-GVA global apparent power. Also, a real reinforcement situation has also been considered. A new HVDC link of 230-km length and 1000-MW power capacity is placed as shown in Figure 12 and according to Midi-Provence project [27]. The objective is to control this DC link.

As before, the new H_∞ controller obtained in this case is compared with the standard vector controller. Figure 13(a) and (b) give the responses of active and reactive powers to a symmetrical short circuit applied at one of the HVDC terminals in the Fos area (Figure 12), cleared after 100 ms. One can observe, as for the previous France–Spain case, that the dynamic behavior is better with the new controller also on this new large-scale benchmark. This is confirmed by the analysis of the transient stability of the zone. In fact, Table VI shows that the CCT is augmented when the new control is used.

7. CONCLUSION

A new method for synthesizing the controllers of HVDC converters was proposed in this paper. It is based on the use of an enriched control model that takes into consideration the dynamics that impact the stability of the neighbor zone of the link. In particular, a new type of interaction of distant machines was put into evidence by defining electrical coupling modes. These dynamics are captured by both linear and nonlinear considerations. To take advantage from the robust theory, the topology variations, which correspond to the main dynamics of the control model, have been

treated as uncertainties in an H_∞ synthesis. However, other kinds of control, even nonlinear, can be envisaged. From this point of view, the methodology presented here is an open control framework, which allows to

- directly take into account the neighbor zone of the HVDC link considering the dynamics that are stringent for the transient stability and thus improve the latter,
- coordinate the control actions of the two converters,
- obtain better performances than the standard controllers.

The synthesis of the control model and of the regulator is implementable in a large scale. This was proven in the paper by treating a concrete actual European grid reinforcement case. Moreover, this framework is adequate for the coordination of the control action of several close HVDC links or of the latter with other actuators like generators. This point will be treated in a forthcoming work.

APPENDIX A: SOLUTION OF THE H_∞ CONTROL PROBLEM

A.1. The system's representation

The stationary linear system can be given by its state representation:

$$\begin{cases} \dot{x}(t) = Ax(t) + Bu(t) \\ y(t) = Cx(t) + Du(t). \end{cases} \tag{A.1}$$

The transfer matrix of this system is

$$P(s) = C(sI - A)^{-1}B + D \tag{A.2}$$

and is noted $P = \left[\begin{array}{c|c} A & B \\ \hline C & D \end{array} \right]$.

The controller $K(s)$ and the uncertainties of $G(s)$ can be put into evidence according to Figure A.1, where $G(s)$ is the generalized process (the process $P(s)$ augmented with the weights), $K(s)$ is the controller, $\Delta(s)$ is the uncertainty modeling, w is exogenous entries of the system, z is the errors between references and outputs of the system, y is the measured outputs, and u is the control signals.

This representation is called standard form of the system and generates an augmented system described by a differential equation and two output equations:

$$\begin{cases} \dot{x}(t) = Ax(t) + B_1w(t) + B_2u(t) \\ z(t) = C_1x(t) + D_{11}w(t) + D_{12}u(t) \\ y(t) = C_2x(t) + D_{21}w(t) + D_{22}u(t), \end{cases} \tag{A.3}$$

$$G = \left[\begin{array}{c|cc} A & B_1 & B_2 \\ \hline C_1 & D_{11} & D_{12} \\ C_2 & D_{21} & D_{22} \end{array} \right]. \tag{A.4}$$

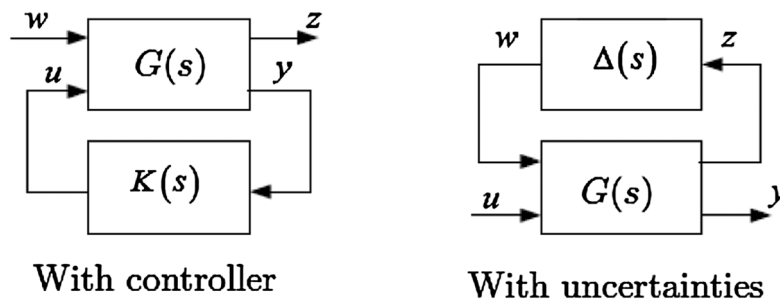


Figure A.1. Standard form representation of a system.

The transfer matrix $G(s)$ of this augmented system can be partitioned according to the inputs/outputs

$$G(s) = \begin{bmatrix} G_{11}(s) & G_{12}(s) \\ G_{21}(s) & G_{22}(s) \end{bmatrix}. \tag{A.5}$$

A.2. Problem formulation

The plant G has two inputs, the exogenous input w , which includes reference signal and disturbances; and the control variables u . There are two outputs, the error signals z , which we want to minimize; and the measured variables y , which we use to control the system. y is used in K to calculate the control variable u .

It is possible to express the dependency of z on w as $z = F_l(P, K)w$,

$$F_l(P, K) = G_{11} + G_{12}K(I - G_{22}K)^{-1}G_{21}, \tag{A.6}$$

called the lower linear fractional transformation.

The objective of the H_∞ control design is to find a controller K , which stabilizes the closed loop for all the plants in the family $P_\Delta(s)$ and such that $F_l(P, K)$ is minimized according to the H_∞ norm. The infinity norm of the transfer function matrix is defined as

$$\|F_l(P, K)\|_\infty = \sup_{\omega} \bar{\sigma}(F_l(P, K)(j\omega)),$$

where $\bar{\sigma}$ is the maximum singular value of the matrix $F_l(P, K)(j\omega)$.

Because the H_∞ norm to be minimized is a superior value over ω of the maximum singular value $\bar{\sigma}$ of the transfer $F_l(P, K)(j\omega)$, this allows us to develop a controller that takes into consideration the worst-case situation.

Notice that the singular values are used for in the case of multivariable systems to represent the model gains over all input and output directions.

A.3. Solution of the H_∞ control problem

Consider the generalized state representation described by (A.3) and (A.4) and its transfer matrix given by (A.5). We assume that $D_{22} = 0$. That is, it does not exist any direct transmission from the input to the output.

The solution of the problem is based on the solution of the algebraic Riccati equation as it is detailed in the Appendix A,

$$XE + E^T X - XWX + Q = 0, \tag{A.7}$$

with $W = W^T$ and $Q = Q^T$.

A stabilizing solution X of (A.7), if it exists, is a symmetrical matrix such that $(E-WX)$ is a stable matrix (eigenvalues with strictly negative real parts). This solution is noted:

$$X = Ric \begin{pmatrix} E & -W \\ -Q & -E^T \end{pmatrix}. \tag{A.8}$$

The solution of the Riccati equation is as follows:

Let be $R_n = D_{1*}^T D_{1*} - \begin{bmatrix} \gamma^2 I_{m1} & 0 \\ 0 & 0 \end{bmatrix}$ and $\tilde{R}_n = D_{*1} D_{*1}^T - \begin{bmatrix} \gamma^2 I_{p1} & 0 \\ 0 & 0 \end{bmatrix}$,

where $D_{1*} = \begin{bmatrix} D_{11} & D_{12} \end{bmatrix}$ and $D_{*1} = \begin{bmatrix} D_{11} \\ D_{21} \end{bmatrix}$.

Because R_n and \tilde{R}_n are not singular, we define the two Hamiltonian matrices

$$H = \begin{bmatrix} A & 0 \\ -C_1^T C_1 & -A^T \end{bmatrix} - \begin{bmatrix} B \\ -C_1^T D_{1*} \end{bmatrix} R_n^{-1} \begin{bmatrix} D_{1*}^T C_1 & B^T \end{bmatrix}, \tag{A.9}$$

$$J = \begin{bmatrix} A^T & 0 \\ -B_1 B_1^T & -A \end{bmatrix} - \begin{bmatrix} C^T \\ -B_1 D_{*1}^T \end{bmatrix} \tilde{R}_n^{-1} \begin{bmatrix} D_{*1} B_1^T & C \end{bmatrix}. \tag{A.10}$$

If we put $X = Ric(H)$ and $Y = Ric(J)$, we can define the two matrices

$$F = -R_n^{-1} (D_{1*}^T C_1 + B^T X) = \begin{bmatrix} F_1 \\ F_2 \end{bmatrix} = \begin{bmatrix} F_{11} \\ F_{12} \\ F_2 \end{bmatrix}, \tag{A.11}$$

$$L = -(B_1 D_{*1}^T + Y C^T) \tilde{R}_n^{-1} = [L_1 \ L_2] = [L_{11} \ L_{12} \ L_2], \tag{A.12}$$

where F_1, F_2, F_{11} , and F_{12} are formed respectively by $m_1, m_2, m_1 - p_2$, and p_2 lines and L_1, L_2, L_{11} , and L_{12} are formed respectively by $p_1, p_2, p_1 - m_2$, and m_2 columns.

A solution exists if the two following conditions are satisfied:

- (A, B_2) is stabilizable, and (C_2, A) is detectable;
- $D_{12} = \begin{bmatrix} 0 \\ I_{m_2} \end{bmatrix}$ and $D_{21} = [0 \ I_{p_2}]$ are then respectively of rank m_2 and p_2 ;
- $\forall \omega \in \mathbb{R} \text{ rang} \begin{bmatrix} A - j\omega I_n & B_2 \\ C_1 & D_{12} \end{bmatrix} = n + m_2$; then this matrix is of full rank; in addition, P_{12} has no invariant zeros on the imaginary axis;
- $\forall \omega \in \mathbb{R} \text{ rang} \begin{bmatrix} A - j\omega I_n & B_1 \\ C_2 & D_{21} \end{bmatrix} = n + p_2$; then this matrix is of full rank; in addition, P_{21} has no invariant zeros on the imaginary axis.

Let $D_{11} = \begin{bmatrix} D_{1111} & D_{1112} \\ D_{1121} & D_{1122} \end{bmatrix}$ with D_{1122} is of dimension $m_2 \times p_2$; the solution will be given by the following theorem :

Theorem 1

If a system $G(s)$ verifies the hypotheses 1–4 described earlier, then

- (a) it exists a controller $K(s)$, which stabilizes the closed loop and such that $\|F_l(P, K)\|_\infty < \gamma$ if and only if
 1. $\gamma > \max(\bar{\sigma}[D_{1111} \ D_{1112}], \bar{\sigma}[D_{1111} \ D_{1121}])$,
 2. it exists solutions $X \geq 0$ and $Y \geq 0$, which verify the two Riccati equations relating to Hamiltonians matrices H and J and such that $\rho(XY) < \gamma^2$, where $\rho(\cdot)$ designs the spectral radius.
- (b) If the conditions of part (a) are satisfied, then the controllers, which stabilize the system and which verify $\|F_l(P, K)\|_\infty < \gamma$, are given by

$$K(s) = F_l(M, \phi), \tag{A.13}$$

where $\|\phi(s)\|_\infty < \gamma$ and

$$M = \left[\begin{array}{c|cc} \hat{A} & \hat{B}_1 & \hat{B}_2 \\ \hline \hat{C}_1 & \hat{D}_{11} & \hat{D}_{12} \\ \hat{C}_2 & \hat{D}_{21} & 0 \end{array} \right] \tag{A.14}$$

and

$$\begin{aligned} \hat{D}_{11} &= -D_{1121} D_{1111}^T (\gamma^2 I_{m_1-p_2} - D_{1111} D_{1111}^T)^{-1} D_{1112} - D_{1122} \\ \hat{D}_{12} &\in \mathbb{R}^{m_2 \times m_2} \text{ and } \hat{D}_{21} \in \mathbb{R}^{p_2 \times p_2} \text{ are two arbitrary matrices that verify} \\ \hat{D}_{12} \hat{D}_{12}^T &= I_{m_2} - D_{1121} (\gamma^2 I_{m_1-p_2} - D_{1111}^T D_{1111})^{-1} D_{1121}^T \\ \hat{D}_{21}^T \hat{D}_{21} &= I_{p_2} - D_{1121}^T (\gamma^2 I_{p_1-m_2} - D_{1111} D_{1111}^T)^{-1} D_{1121} \\ \hat{B}_2 &= Z(B_2 + L_{12}) \hat{D}_{12} \text{ and } \hat{B}_1 = -Z L_2 + Z(B_2 + L_{12}) \hat{D}_{11} \\ \hat{C}_2 &= -\hat{D}_{21} (C_2 + F_{12}) \text{ and } \hat{C}_1 = F_2 - \hat{D}_{11} (C_2 + F_{12}) \\ Z &= (I_n - \gamma^{-2} Y X)^{-1} \\ \hat{A} &= A + B F - \hat{B}_1 (C_2 + F_{12}). \end{aligned}$$

The controller calculated for $\phi(s) = 0$ is called the central corrector; it is generally used under the form

$$K(s) = \begin{bmatrix} \hat{A} & \hat{B}_1 \\ \hat{C}_1 & \hat{D}_{11} \end{bmatrix}. \quad (\text{A.15})$$

APPENDIX B: FORM OF THE CONTROL MODEL P(S)

$$P_{11}(s) = \frac{814.6s^{28} + 2.44810^6s^{27} + 2.45810^9s^{26} + 8.2810^{11}s^{25} + 4.7710^{12}s^{24} + 1.710^{14}s^{23} + 8.0210^{14}s^{22}}{s^{29} + 1006s^{28} + 6.0210^6s^{27} + 14.03610^9s^{26} + 1.02310^{12}s^{25} + 6.0910^{12}s^{24} + 2.110^{14}s^{23} + 1.0110^{15}s^{22} + 1.8110^{16}s^{21}} \\ \frac{1.4610^{16}s^{21} + 8.9210^{16}s^{20} + 7.03910^{17}s^{19} + 2.45610^{18}s^{18} + 2.07410^{19}s^{17} + 6.27910^{19}s^{16} + 3.9310^{20}s^{15} + 1.9310^{21}s^{14} + 4.8510^{21}s^{13}}{7.4210^{16}s^{20} + 8.6910^{17}s^{19} + 3.0710^{18}s^{18} + 2.5610^{19}s^{17} + 7.84510^{19}s^{16} + 4.810^{20}s^{15} + 1.2810^{21}s^{14}} \\ \frac{1.0810^{22}s^{12} + 3.8710^{22}s^{11} + 7.2410^{22}s^{10} + 1.9310^{23}s^9 + 2.89410^{23}s^8 + 5.60710^{23}s^7 + 6.21210^{23}s^6 + 8.4110^{23}s^5 + 5.7910^{23}s^4 + 5.1210^{23}s^3}}{610^{21}s^{13} + 1.35810^{22}s^{12} + 4.78110^{22}s^{11} + 9.0710^{22}s^{10} + 2.3710^{23}s^9 + 3.6210^{23}s^8 + 6.8710^{23}s^7 + 7.7610^{23}s^6 + 1.0210^{24}s^5 + 7.15410^{23}s^4 + 6.110^{23}s^3} \\ \frac{1.7710^{23}s^2 + 6.6310^{22}s + 7.2510^{21}}{2.0910^{23}s^2 + 7.4910^{22}s + 2.6110^{21}}.$$

ACKNOWLEDGEMENTS

The authors would like to thank Prof. Eric Monmasson, University of Cergy-Pontoise; Dr Alexandre Parisot, head of Integration of New Technology division (INT) of RTE; and Patrick Panciatici, scientific advisor at RTE-DES, for the helpful suggestions and remarks.

REFERENCES

1. Hingorani GN, Gyugyi L. *Understanding FACTS: Concepts and Technology of Flexible AC Transmission Systems*. IEEE Press: Piscataway, 2000.
2. Goodrich F, Andersen B. The 2000 MW HVDC link between England and France. *Power Engineering Journal* 1987; **1**(2):69–74.
3. Hauer JF. Robustness issues in stability control of large electric power systems. *Proceedings of 32nd IEEE Conference on Decision and Control*, San Antonio, Texas, 1993; 2329–2334.
4. Vovos NA, Galanos GD. Enhancement of the transient stability of integrated AC/DC systems using active and reactive power modulation. *IEEE Power Engineering Review* 1985; **5**(7):33–34.
5. Smed T, Andersson G. Utilizing HVDC to damp power oscillations. *IEEE Transactions on Power Delivery* 1993; **8**(2):620–627.
6. Hammad AE, Gagnon J, McCallum D. Improving the dynamic performance of a complex AC/DC system by HVDC control modifications. *IEEE Transactions on Power Delivery* 1990; **5**(5):1934–1943.
7. Shun FL, Muhamad R, Srivastava K, Cole S, Hertem DV, Belmans R. Influence of VSC HVDC on transient stability: case study of the Belgian grid. *Proceedings of IEEE Power and Energy Society General Meeting*, Minneapolis, USA, 2010; 1–7.
8. Taylor CW, Lefebvre S. HVDC controls for system dynamic performance. *IEEE Transactions on Power Systems* 1991; **6**(2):743–752.
9. Hu Z, Mao C, Lu J. Improvement of transient stability in AC system by HVDC Light. *Proceedings of Transmission and Distribution Conference and Exhibition IEEE*, Dalian, 2005; 1–5.
10. Mao C, Hu Z, Lu J, Chang D, Fan S. Application of an optimal coordinated control strategy to VSC HVDC. *Proceedings of Power Systems Conference and Exposition IEEE*, Atlanta, 2006; 2141–2145.
11. To K, David A, Hammad A. A robust co-ordinated control scheme for HVDC transmission with parallel AC systems. *IEEE Transactions on Power Delivery* 1994; **9**(3):1710–1716.
12. Latorre H, Ghandhari M. Improvement of power system stability by using a VSC-HVDC. *International Journal of Electrical Power & Energy Systems* 2011; **33**(2):332–339.
13. Fuchs A, Imhof M, Demiray T, Morari M. Stabilization of large power systems using VSC-HVDC and model predictive control. *IEEE Transactions on Power Delivery* 2014; **29**(1):480–488.
14. Rostamkolai N, Phadke AG, Long WF, Thorp JS. An adaptative optimal control strategy for dynamic stability enhancement of AC/DC power systems. *IEEE Transactions on Power Systems* 1988; **3**(3):1139–1145.
15. Kundur P. *Power Stability and Control*. McGraw-Hill: New York, 1994.
16. Aouini R, Ben Kilani K, Marinescu B, Elleuch M. Improvement of fault critical time by HVDC transmission. *In Proceedings of Systems, Signals and Devices*, Sousse, Tunisia, 2011; 1–6.
17. Ramaswamy GN, Verghese GC, Rouco L, Vialas C, Demarco CL. Synchrony, aggregation and multi-area eigenanalysis. *IEEE Transaction on Power Systems* 1995; **10**(4):1986–1993.
18. Luther M, Biernaka I, Preotescu D. Feasibility aspects of a synchronous coupling of the IPS/UPS with the UCTE. *Water and Energy International* 2012; **69**(3):62–62.
19. Breulmann H, Grebe E, L?sing M. Analysis and damping of inter-area oscillations in the UCTE/CENTREL power system. *CIGRE Session*, Paris, 2000; 38–113.

20. Baldwin TL, Mili L, Phadke AG. Dynamic ward equivalents for transient stability analysis. *IEEE Transactions on Power Systems* 1994; **9**(1):59–67.
21. Latorre HF, Ghandhari M, Söder L. Active and reactive power control of a VSC-HVDC. *Electric Power Systems Research* 2008; **78**(10):1756–1763.
22. Meyer B, Stubbe M. EUROSTAG, a single tool for power system simulation. *Transmission & Distribution International*, Brussels, Belgium, 1992; 47–52.
23. Zhou K, Doyle JC. *Essentials of Robust Control*. Prentice Hall: New Jersey, 1997.
24. Skogestad S, Postlethwaite I. *Multivariable Feedback Control*. John Wiley: Chichester, 1996.
25. Li S, Haskew TA, Xu L. Control of HVDC light system using conventional and direct current vector control approaches. *IEEE Transactions on Power Electronics* 2010; **25**(12):3106–3118.
26. Kwakernaak H, Sivan R. *Linear Optimal Control systems*. John Wiley: New York, 1972.
27. Schéma décennal de développement du réseau, 2013. (Available from: <http://www.rte-france.com/>).